International Journal of Non-Linear Mechanics 47 (2012) 118–128

Contents lists available at SciVerse ScienceDirect

International Journal of Non-Linear Mechanics

journal homepage: www.elsevier.com/locate/nlm

Coupled thermo-mechanical analysis of shape memory alloy circular bars in pure torsion

Reza Mirzaeifar [a], Reginald DesRoches [b], Arash Yavari [b,*], Ken Gall [a,c]

[a] George W. Woodruff School of Mechanical Engineering, Georgia Institute of Technology, Atlanta, GA 30332, USA
[b] School of Civil and Environmental Engineering, Georgia Institute of Technology, Atlanta, GA 30332, USA
[c] School of Materials Science and Engineering, Georgia Institute of Technology, Atlanta, GA 30332, USA

ARTICLE INFO

Article history:
Received 27 April 2011
Received in revised form
12 December 2011
Accepted 26 January 2012
Available online 4 February 2012

Keywords:
Torsion
Shape memory alloy
Thermo-mechanical coupling
Rate-dependent
Ambient conditions

ABSTRACT

Pure torsion of shape memory alloy (SMA) bars with circular cross section is studied by considering the effect of temperature gradient in the cross sections as a result of latent heat generation and absorption during forward and reverse phase transformations. The local form of energy balance for SMAs by taking into account the heat flux effect is coupled to a closed-form solution of SMA bars subjected to pure torsion. The resulting coupled thermo-mechanical equations are solved for SMA bars with circular cross sections. Several numerical case studies are presented and the necessity of considering the coupled thermo-mechanical formulation is demonstrated by comparing the results of the proposed model with those obtained by assuming an isothermal process during loading–unloading. Pure torsion of SMA bars in various ambient conditions (free and forced convection of air, and forced convection of water flow) subjected to different loading–unloading rates are studied and it is shown that the isothermal solution is valid only for specific combinations of ambient conditions and loading rates.

1. Introduction

Shape memory alloys (SMAs) in recent applications are usually subjected to combined loadings in contrast with the early devices that were mostly designed based on using the uniaxial deformation of SMA wires operating as tendons. The recent interest in using sophisticated SMA devices reveals the necessity of analyzing these materials subjected to complicated loadings. There are numerous industrial applications using SMA helical springs as active actuators [17,6]. In addition to actuators, it has been shown recently that due to the hysteretic response of SMAs, helical springs made of these materials can be efficiently used as energy dissipating devices for improving the response of structures subjected to earthquake loads [30]. Speicher et al. [30] studied SMA helical springs subjected to cyclic loads and it was shown that Nitinol helical springs are efficient devices for damping in a vast range of structures besides their ability in minimizing the residual deformations after an earthquake. It is well known that for most practical helical springs (when the ratio of the mean coil radius to the cross section radius is large and the helix angle is small), assuming that each portion of a spring acts as a straight bar under torsion gives accurate results [32]. The application of torsion analysis for studying the behavior of SMA helical springs motivated the authors to seek accurate and efficient analysis techniques for the pure torsion of SMA bars with circular cross sections. There are a few attempts to study the torsion problem for SMA bars in the literature by using numerical methods or considering simplified SMA constitutive relations (see [20,22] for a comprehensive review of the available solutions for torsion of SMA bars). An accurate three-dimensional phenomenological constitutive equation is reduced for studying the one-dimensional pure torsional problem and exact solutions are proposed for analyzing the torsion of straight SMA bars [20] and SMA curved bars and helical springs [22]. In these studies, it is assumed that the material temperature is not affected by the phase transformation and it remains uniformly distributed and equal to the initial temperature during loading–unloading. However, it is well known that the phase transformation in SMAs is accompanied by heat generation during austenite to martensite (forward) and heat absorption during martensite to austenite (reverse) phase transformation [16,2,27]. Assuming a constant temperature is identical to assuming an isothermal process that requires some particular ambient conditions, geometric properties, and loading rates to allow the material to exchange all the phase transformation latent heat with the ambient during loading–unloading. In a recent study, we have shown that in the case of SMA wires and bars subjected to uniaxial loads, response of the material is strongly affected by the thermo-mechanical coupling in SMAs [21]. In Mirzaeifar et al. [21], the heat balance equation that accounts for the phase transformation heat and the heat flux are

* Corresponding author.
E-mail address: arash.yavari@ce.gatech.edu (A. Yavari).

0020-7462/$ - see front matter © 2012 Elsevier Ltd. All rights reserved.
doi:10.1016/j.ijnonlinmec.2012.01.007

coupled to the uniaxial constitutive relation of SMAs. Our formulation can be used for SMA wires and bars with circular cross sections subjected to different uniaxial loading–unloading rates in various ambient conditions. The accuracy of the proposed coupled formulation was validated using experimental results. We have shown that the accuracy of assuming adiabatic or isothermal conditions in the tensile response of SMA bars strongly depends on the size and the ambient conditions in addition to the rate-dependency. We concluded that for having an analysis with acceptable accuracy, a coupled thermo-mechanical formulation is inevitable.

To our best knowledge, there is no reported work in the literature on studying the coupled thermo-mechanical response of SMA bars in torsion. In this paper, we present the heat balance equation by considering the phase transformation latent heat and the heat flux effects for bars in pure torsion. This relation is coupled with the exact solution for pure torsion of SMA bars that we presented previously assuming that the SMA bar is under torsion in a constant temperature [20,22]. The generation and absorption of latent heat due to phase transformation and its flux toward the other parts of the cross section in which the material is responding elastically is taken into consideration. Boundary conditions at the outer surface of the bar caused by free or forced convection of air or fluid flow are carefully enforced. For verification purposes the results of the present coupled thermo-mechanical formulation are compared with the experimental data for a thin-walled NiTi tube subjected to pure torsion.

Since the heat conduction inside the SMA bar and the convection with the ambient both are strongly affected by the loading rate, it is shown that the response of SMA bars in torsion is rate dependent. Several case studies are considered and the effect of loading rate and ambient conditions on the torsional response of SMA bars is studied in detail. In each case, the results are compared with the solution obtained by ignoring the thermo-mechanical coupling, and it is shown that the special characteristics of torsion in SMA bars leads to a significant difference between the isothermal and coupled thermo-mechanical results. It is worth noting that although some simplified lumped temperature methods can be used for studying the coupled thermo-mechanical response of SMA bars subjected to uniaxial loading in particular conditions (when there are no propagating transformation fronts along the length, the Biot number is sufficiently small, and thermal boundary conditions at the ends are insulated), due to the non-uniform distribution of shear stress in the cross section of SMA bars subjected to torsion, the effect of temperature non-uniformity and the flux of latent heat is more evident compared to the simple tension without propagating phase fronts.

This paper is organized as follows. In Section 2 a three-dimensional coupled thermo-mechanical formulation for SMAs is briefly explained. The reduction of the model to the one-dimensional pure torsion and the exact solution for SMA bars with circular cross section in torsion is presented in Section 3. Section 4 contains several case studies and some important observations regarding the torsional response of SMA bars for different loading rates and boundary conditions. Section 5 presents a study of the effect of various parameters (loading rate, size, and ambient condition) on the temperature distributions in the cross section. Conclusions are given in Section 6.

2. Coupled thermo-mechanical governing equations for SMAs

Deriving the three-dimensional coupled thermo-mechanical governing equations for SMAs is explained in details in Mirzaeifar et al. [21]. Starting from the first law of thermodynamics in local form and using the second law of thermodynamics, the following coupled energy balance equation is obtained [16]

$$T\boldsymbol{\alpha}:\dot{\boldsymbol{\sigma}}+\rho c\dot{T}+\left[-\pi+T\Delta\boldsymbol{\alpha}:\boldsymbol{\sigma}-\rho\Delta c\ T\ln\left(\frac{T}{T_0}\right)+\rho\Delta s_0 T\right]\dot{\xi}=-\mathrm{div}\,\boldsymbol{q}+\rho\hat{g}, \tag{1}$$

where T is the absolute temperature, $\boldsymbol{\alpha},\rho,c$ and s_0 are the effective thermal expansion coefficient tensor, density, effective specific heat, and specific entropy, respectively. The symbols $\boldsymbol{\sigma}$ and T_0 denote the Cauchy stress tensor and reference temperature. It is worth noting that, although the constitutive relations are capable of modeling finite strains [26], we consider the small strains assumption and the formulation is not affected by the stress measure in use. The parameter ξ is the martensitic volume fraction, the terms $\boldsymbol{q}$ and $\hat{g}$ account for the heat flux and any internal heat generation except the phase transformation induced generated heat. Dot on a quantity $(\cdot)$ denotes time derivative and any effective material property $\mathbf{P}$ is assumed to vary with the martensitic volume fraction as $\mathbf{P}=\mathbf{P}^A+\xi\Delta\mathbf{P}$, where the superscript A denotes the austenite phase and the symbol $\Delta(\cdot)$ denotes the difference of a quantity $(\cdot)$ between the martensitic and austenitic phases, i.e. $\Delta(\cdot)=(\cdot)^M-(\cdot)^A$ with M denoting the martensite phase. The term π in (1) is the thermodynamic force conjugate to the martensitic volume fraction and depends on the chosen definition for the free energy. In this paper we use the Gibbs free energy for polycrystalline SMAs [1,26] and this leads to the following thermodynamic force (see [26] for details of deriving this term):

$$\pi=\boldsymbol{\sigma}:\boldsymbol{\Gamma}+\frac{1}{2}\boldsymbol{\sigma}:\Delta\mathbb{S}:\boldsymbol{\sigma}+\Delta\boldsymbol{\alpha}:\boldsymbol{\sigma}(T-T_0)-\rho\Delta c\left[(T-T_0)-T\ln\left(\frac{T}{T_0}\right)\right]+\rho\Delta s_0 T-\frac{\partial f}{\partial\xi}-\rho\Delta u_0, \tag{2}$$

where $\boldsymbol{\Gamma}$ is the transformation tensor, $\mathbb{S}$ and u_0 are the compliance tensor and the specific internal energy at the reference state. The function $f(\xi)$ is a hardening function that models the transformation strain hardening in the SMA material. Using this thermodynamic force, the second law of thermodynamics in the form of a dissipation inequality can be written as $\pi\dot{\xi}\geq 0$. This inequality is then used to obtain the conditions that control the onset of forward and reverse phase transformations as

$$\Phi=0,\quad \Phi=\begin{cases}\pi-Y, & \dot{\xi}>0,\\ -\pi-Y, & \dot{\xi}<0,\end{cases} \tag{3}$$

where Y is a threshold value for the thermodynamic force during phase transformation [26]. The consistency during phase transformation guaranteeing the stress and temperature states to remain on the transformation surface is given by $\dot{\Phi}=0$ [28,26]. Substituting (2) and (3) into this consistency condition, the following relation is obtained between the rate of change of martensitic volume fraction, the stress tensor, and temperature

$$\dot{\xi}=-\frac{(\boldsymbol{\Gamma}+\Delta\mathbb{S}:\boldsymbol{\sigma}):\dot{\boldsymbol{\sigma}}+\rho\Delta s_0\dot{T}}{\mathcal{D}^{\pm}}, \tag{4}$$

where $\mathcal{D}^{+}=\rho\Delta s_0(M_s-M_f)$ for the forward phase transformation ($\dot{\xi}>0$) and $\mathcal{D}^{-}=\rho\Delta s_0(A_s-A_f)$ for reverse phase transformation ($\dot{\xi}<0$). The parameters A_s,A_f,M_s,M_f represent the austenite and martensite start and finish temperatures, respectively. Substituting (4) into (1) and assuming $\Delta\alpha=\Delta c=0$ – valid for almost all practical SMA alloys – the following expression is obtained:

$$[T\boldsymbol{\alpha}-\mathcal{F}_1(\boldsymbol{\sigma},T)]:\dot{\boldsymbol{\sigma}}+[\rho c-\mathcal{F}_2(T)]\dot{T}=-\mathrm{div}\,\boldsymbol{q}+\rho\hat{g}, \tag{5}$$

where

$$\mathcal{F}_1(\boldsymbol{\sigma},T)=\frac{1}{\mathcal{D}^{\pm}}(\boldsymbol{\Gamma}+\Delta\mathbb{S}:\boldsymbol{\sigma})(\mp Y+\rho\Delta s_0 T),$$

$$\mathcal{F}_2(T)=\frac{\rho\Delta s_0}{\mathcal{D}^{\pm}}(\mp Y+\rho\Delta s_0 T). \tag{6}$$

In (6) the symbol $(+)$ is used for forward phase transformation and $(-)$ is used for the reverse transformation. Eq. (5) is one of the two coupled relations for describing the thermo-mechanical response of SMAs. The second relation is the constitutive equation and reads [26]

$$\boldsymbol{\epsilon}=\mathbb{S}:\boldsymbol{\sigma}+\boldsymbol{\alpha}(T-T_0)+\boldsymbol{\epsilon}^t, \tag{7}$$

where $\boldsymbol{\epsilon}^t$ is the transformation strain tensor related to the rate of change of martensitic volume fraction by the evolution equation $\dot{\boldsymbol{\epsilon}}^t=\boldsymbol{\Gamma}\dot{\xi}$. In the following section, these coupled relations are simplified for pure torsion.

3. Reduction of the coupled equations for pure torsion

The exact solution for pure torsion of shape memory alloy circular bars ignoring the effect of phase transformation latent heat, and assuming the isothermal condition was given in Mirzaeifar et al. [20,22]. In this paper we modify the solution for the pure torsion of circular bars considering the coupled thermo-mechanical governing equations for SMAs as presented in the previous section and Mirzaeifar et al. [21]. In the new formulation, we study the coupled thermo-mechanical torsion problem in the presence of the phase transformation induced heat generation/absorption and the heat flux effect in the cross section. A finite difference formulation is used to solve the governing coupled thermo-mechanical equations.

3.1. Coupled thermo-mechanical governing equations in torsion of SMA bars

According to Saint-Venant's solution the state of stress and strain is one dimensional and shear strain varies linearly from the central axis toward the outer radius for bars with circular cross sections [11,29]. It is worth noting that the Saint-Venant assumption of no warpage in circular cross sections is a result of symmetry in kinematics and it is independent of the material response. This phenomenon has been shown theoretically for elastic–plastic torsion of prismatic bars with circular cross section [23,14]. Grewe and Kappler [8] reported some tests on the plastic torsion of prismatic bars with circular cross sections and proved the validity of Saint-Venant assumption for a material with strain hardening response. The validity of Saint-Venant assumption for the elastic–plastic torsion has also been studied numerically [31,15]. For a material with phase transformation, comparable to the strain hardening plastic response, we assume that the Saint-Venant assumption is valid for SMA prismatic bars with circular cross sections. The stress, strain, and transformation strain tensors have the following forms:

$$\boldsymbol{\sigma}=\begin{bmatrix}0&0&0\\0&0&\tau_{\theta z}\\0&\tau_{\theta z}&0\end{bmatrix},\quad \boldsymbol{\epsilon}=\begin{bmatrix}0&0&0\\0&0&\epsilon_{\theta z}\\0&\epsilon_{\theta z}&0\end{bmatrix},\quad \boldsymbol{\epsilon}^t=\begin{bmatrix}0&0&0\\0&0&\epsilon^t_{\theta z}\\0&\epsilon^t_{\theta z}&0\end{bmatrix}, \tag{8}$$

where $\tau_{\theta z}$, $\epsilon_{\theta z}$ and $\epsilon^t_{\theta z}$ are the shear stress, shear strain and transformation shear strains, respectively. The no warpage assumption forces the out of plane strains (both the total and transformation strains) to be zero. The transformation strain tensor in (8) is also consistent with the transformation tensor and the evolution equation in Mirzaeifar et al. [20]. The transformation tensors for pure torsion are given as

$$\boldsymbol{\Gamma}^+=\frac{\sqrt{3}}{2}H\,\mathrm{sgn}(\tau_{\theta z})\begin{bmatrix}0&0&0\\0&0&1\\0&1&0\end{bmatrix},\quad \boldsymbol{\Gamma}^-=\frac{\sqrt{3}}{2}H\,\mathrm{sgn}(\epsilon^{tr}_{\theta z})\begin{bmatrix}0&0&0\\0&0&1\\0&1&0\end{bmatrix}, \tag{9}$$

where H is the ultimate transformation strain magnitude for full austenite to martensite transformation in uniaxial loading, $\mathrm{sgn}(\cdot)$ is the sign function, and the superscripts $(+)$ and $(-)$ for $\boldsymbol{\Gamma}$ denote the forward and inverse phase transformations, respectively (see [1] for the reason of assuming different transformation tensors in forward and reverse phase transformations, and [20] for details of deriving these tensors from the three-dimensional case for pure torsion). It is shown by the authors that the shear strain is related to the shear stress in SMA circular bars by the following expression [20,22]:

$$\epsilon_{\theta z}=\frac{1+\nu}{E^A+\xi^{\pm}(\Delta E)}\tau_{\theta z}+\frac{1}{\rho b^{\pm}}\left\{\frac{3}{2}H^2\tau_{\theta z}+\sqrt{3}H\tau^2_{\theta z}\aleph^{\pm}\Delta S_{44}+\frac{\sqrt{3}}{2}H\aleph^{\pm}f^{\pm}(T)\right\}, \tag{10}$$

where ν is Poisson's ratio (assumed to be the same for both phases), E^A and ΔE are the austenite elastic modulus and the elastic modulus difference between martensite and austenite phases, respectively, $\Delta S_{44}=(1/G^M)-(1/G^A)$, where G is the shear modulus, and the other parameters for the forward and reverse phase transformation are $\aleph^+=\mathrm{sgn}(\tau_{\theta z})$, $\aleph^-=\mathrm{sgn}(\epsilon^{tr}_{\theta z})$, $\rho b^+=\rho b^M=-\rho\Delta s_0(M_s-M_f)$, $\rho b^-=\rho b^A=-\rho\Delta s_0(A_f-A_s)$, $f^+(T)=\rho\Delta s_0(T-M_s)$, and $f^-(T)=\rho\Delta s_0(T-A_f)$. The explicit expressions for the martensitic volume fraction in pure torsion are obtained by substituting (8) into (2) and (3) and read

$$\xi^+=\frac{1}{\rho b^M}\{\sqrt{3}H|\tau_{\theta z}|+2\tau^2_{\theta z}\Delta S_{44}+f^+(T)\},$$

$$\xi^-=\frac{1}{\rho b^A}\{\sqrt{3}H\tau_{\theta z}\,\mathrm{sgn}(\epsilon^{tr}_{\theta z})+2\tau^2_{\theta z}\Delta S_{44}+f^-(T)\}. \tag{11}$$

Substituting (11) into (10) and using $\epsilon_{\theta z}=\frac{1}{2}r\theta$, where r is the distance from the axis of the bar and θ is the twist angle per unit length, a quartic equation is obtained for the shear stress. The closed form solution of this equation was presented by the authors and the shear stress was given as a function of the radius, twist angle and temperature, $\tau_{\theta z}=\wp^{\pm}(r,\theta,T)$ [20,22]. This equation will replace the second coupled equation given in (7). The reduction of equation (5) for pure torsion is obtained by substituting (8) and (9) into (5). The set of coupled thermo-mechanical governing equations read

$$\begin{cases}-\tilde{\mathcal{F}}_1(\tau_{\theta z},T)\dot{\tau_{\theta z}}+[\rho c-\tilde{\mathcal{F}}_2(T)]\dot{T}=k\left(\dfrac{\partial^2T}{\partial r^2}+\dfrac{1}{r}\dfrac{\partial T}{\partial r}\right),\\ \tau_{\theta z}=\wp^{\pm}(r,\theta,T),\end{cases} \tag{12}$$

where

$$\tilde{\mathcal{F}}_1(\tau_{\theta z},T)=\frac{1}{\mathcal{D}^{\pm}}(\sqrt{3}H+4\Delta S_{44}\tau_{\theta z})(\mp Y+\rho\Delta s_0T),$$

$$\tilde{\mathcal{F}}_2(T)=\frac{\rho\Delta s_0}{\mathcal{D}^{\pm}}(\mp Y+\rho\Delta s_0T). \tag{13}$$

In $(12)_1$, k is the thermal conductivity and Fourier's law of thermal conduction ($\boldsymbol{q}=-k\boldsymbol{\nabla}T$) is used for deriving the right-hand side. The explicit expression for $(12)_2$ can be found in Mirzaeifar et al. [20]. Temperature and stress distributions at $t=0$ are given as the initial conditions, $T(r,0)=\hat{T}$, $\tau_{\theta z}(r,0)=\hat{\tau}_{\theta z}$. The following boundary conditions are given at the outer surface and the center of the circular bar:

$$k\frac{\partial T(r,t)}{\partial r}\bigg|_{r=R}=h_\infty[T_\infty-T(R,t)],\quad \frac{\partial T(r,t)}{\partial r}\bigg|_{r=0}=0, \tag{14}$$

where h_∞ is the heat convection coefficient, T_∞ is the ambient temperature, and R is the bar outer radius.

3.2. Finite difference discretization of the governing equations

Considering axisymmetric stress and temperature distributions in the circular bar, the set of coupled thermo-mechanical equations (12) and the boundary conditions (14) are discretized by dividing the bar into N_r annuli of equal size Δr and using an explicit finite difference method. The finite difference form of the coupled thermo-mechanical equations (12) for pure torsion is given by (see [21] for details of deriving similar relations in the uniaxial case)

$$\left[-\frac{1}{\mathcal{D}^{\pm}}(\sqrt{3}H+4\Delta S_{44}\tau^n_{\theta z,i})(\mp Y+\rho\Delta s_0 T^n_i)\right]\frac{\tau^{n+1}_{\theta z,i}-\tau^n_{\theta z,i}}{\Delta t}$$
$$+\left[\rho c-\frac{\rho\Delta s_0}{\mathcal{D}^{\pm}}(\mp Y+\rho\Delta s_0 T^n_i)\right]\frac{T^{n+1}_i-T^n_i}{\Delta t}$$
$$=\left(r_i+\frac{\Delta r}{2}\right)\frac{T^n_{i+1}-T^n_i}{r_i(\Delta r)^2}-\left(r_i-\frac{\Delta r}{2}\right)\frac{T^n_i-T^n_{i-1}}{r_i(\Delta r)^2}, \tag{15}$$

$$\tau^{n+1}_{\theta z,i}=\wp^{\pm}(r,\theta^{n+1},T^{n+1}), \tag{16}$$

where the subscript i denotes the ith node in the cross section and the superscript n refers to the nth time increment. For calculating the finite difference approximation of the boundary conditions that include internal heat generation, energy balance for a volume attached to boundary nodes should be considered. For the central node $i=1$, consider a cylindrical volume with radius $\Delta r/2$. The axis of this volume coincides with the bar axis. The finite difference approximation of the boundary condition in the central node is given by [24]

$$k\frac{T^n_2-T^n_1}{2}+\frac{1}{8}(\Delta r)^2\Re^n_1=\frac{1}{8}(\Delta r)^2\rho c\frac{T^{n+1}_1-T^n_1}{\Delta t}, \tag{17}$$

and for the outer node with the convection boundary condition, considering a cylindrical volume attached to the outer node (Mth node) with inner radius $R-\Delta r/2$ and outer radius R, the energy balance gives

$$Rh_\infty(T_\infty-T^n_M)+k\left(R-\frac{\Delta r}{2}\right)\frac{T^n_{M-1}-T^n_M}{\Delta r}+\left[\frac{R\Delta r}{2}-\frac{(\Delta r)^2}{4}\right]\Re^n_M$$
$$=\left[\frac{R\Delta r}{2}-\frac{(\Delta r)^2}{4}\right]\rho c\frac{T^{n+1}_M-T^n_M}{\Delta t}, \tag{18}$$

where the parameters $\Re^n_1$ and $\Re^n_M$ are the equivalent internal heat generation due to phase transformation calculated at the central ($i=1$) and outer ($i=M$) nodes of a bar subjected to torsion as (see [21] for details of deriving similar terms in the uniaxial case)

$$\Re^n_i=\left[-\frac{1}{\mathcal{D}^{\pm}}(\sqrt{3}H+4\Delta S_{44}\tau^n_{\theta z,i})(\mp Y+\rho\Delta s_0 T^n_i)\right]\frac{\tau^{n+1}_{\theta z,i}-\tau^n_{\theta z,i}}{\Delta t}$$
$$+\left[-\frac{\rho\Delta s_0}{\mathcal{D}^{\pm}}(\mp Y+\rho\Delta s_0 T^n_i)\right]\frac{T^{n+1}_i-T^n_i}{\Delta t}. \tag{19}$$

The solution procedure is as following: the stress and temperature in all nodes are known at the nth loading increment (from the initial conditions if $n=0$, and from the completed solution in the previous increment if $n\neq 0$). For any of the nodes except the central and outer nodes, substituting (16) into (15) a non-linear algebraic equation is obtained with only one unknown: T^{n+1}_i, $i=2,\ldots,M-1$. This equation is solved numerically [7] and the temperature at the $(n+1)$th time increment is calculated. Substituting the calculated temperature into (16) gives the stress for the $(n+1)$th increment. For the central and outer nodes, a similar procedure is used considering (16)–(19).

4. Numerical results

We previously reported the exact solution for SMA straight bars with circular cross sections in torsion [20] and SMA helical springs by using the torsion of straight and curved SMA bars [22]. It is worth noting that for springs with very low helix indices, the no warpage assumption is not valid and an appropriate modification is needed for using the torsion theory in analyzing such springs [10]. In a previous work we showed that considering an isothermal process in uniaxial loading–unloading of SMA bars and wires gives accurate results only for wires with small diameters subjected to loadings applied with a very slow rate [21]. To consider the effect of ambient condition, loading rate, and size accurately, it is necessary to solve the coupled thermo-mechanical equations. In this section we study the pure torsion of SMA circular bars using the coupled thermo-mechanical equations of Sections 2 and 3. The present formulation has the capability of considering an accurate convection boundary condition on the bar surface. The details of calculating the convection coefficient on the surface of a cylindrical bar in free air, flowing air, and fluid flow is presented in Mirzaeifar et al. [21].

4.1. Verification using experimental results

There are some reported experiments in the literature for the torsion of prismatic solid SMA bars [5]. However, although these works report the results of torsion tests, the material properties needed in our constitutive model are not presented. Also, the temperature is not measured in these tests. In order to verify our coupled thermo-mechanical formulation the experimental data reported by Lim and McDowell [19] is used. Lim and McDowell [19] performed experiments on thin-wall tubes of pseudoelastic NiTi subjected to pure torsion. During loading–unloading the change of temperature due to latent heat generation/absorption during phase transformation was measured using four thermocouples attached to the specimen and temperature versus shear strain was reported. The specimen was made of a NiTi alloy with the near equiatomic composition and was subjected to a heat treatment after machining from bar stock. In Lim and McDowell [19] only the austenite finish temperature is reported and the other material properties are not measured. However, the results of several uniaxial loading tests are reported that can be used for calibrating the required material constants in the constitutive relation that we are using in this paper. The experimental data in Lim and McDowell [19] and Lim [18] are used for obtaining the following properties (see [26] for details of calibrating the model using experimental data): $E^A=72$ GPa, $E^M=30$ GPa, $\nu^A=\nu^M=0.42$, $H=0.05$, $\rho\Delta s_0=-0.57\times10^6$ J/(m^3 K), $A_f=273.1$ K, $A_s=265.7$ K, $M_f=231.8$ K, $M_s=247.9$ K. Since the thermal conductivity and the specific heat are not reported for this material, we use the previously reported values in the literature for $Ni_{50}Ti_{50}$ [16]: $k=18$ W/(m K), $\rho c^A=\rho c^M=3.9\times10^6$ J/(m^3 K). Both the inner and outer surfaces of the tube are subjected to free convection by air. In the numerical simulations, both the inner and outer nodes are considered as the boundary nodes and the boundary condition (18) is imposed for both these nodes. The thickness is divided into 20 sections. The free convection coefficient for both surfaces is $h_\infty=5.2$ W/m^2 K (see Section 5 in [21] for calculation details). The initial and ambient temperatures are $\hat{T}=T_\infty=287$ K. The loading rate is $\dot{\epsilon}_{eq}=5\times10^{-4}$ s^{-1}, where $\epsilon_{eq}=\gamma/\sqrt{3}=2\epsilon_{\theta z}/\sqrt{3}$ is the Mises equivalent strain. The specimen was subjected to five loading cycles with the equivalent strains between $\pm3\%$. We use the results of the second loading–unloading cycle, in which the material response is stabilized, for verification purposes (due to the unknown thermal condition between the specimen and the grips, the simulation results may be inaccurate for the final cycles

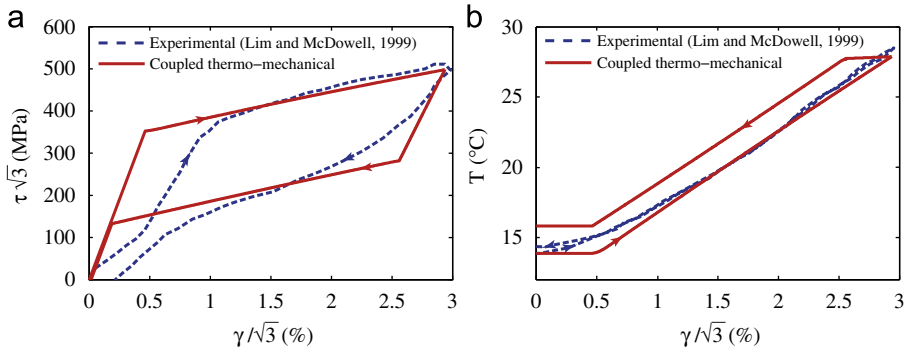

Fig. 1. Comparison of the experimental and analytical results for (a) equivalent shear stress versus equivalent shear strain, and (b) temperature versus equivalent shear strain at the outer surface of a thin-walled SMA tube subjected to pure torsion.

and the second cycle is chosen because the material response is stabilized while the effect of head exchange between the grips and the specimen is minimum). The equivalent shear stress versus the equivalent shear strain at the outer surface obtained from the present formulation is compared with the experimental results in Fig. 1(a). The temperature versus the equivalent shear strain is calculated using the method of this paper and compared with the experimental results in Fig. 1(b). It is worth noting that due to the small thickness (t=1.95 mm), the temperature gradient in the cross section is negligible. We present a detailed study of the effect of size on the temperature gradient in the sequel. As it is shown, the results are in an acceptable agreement. The differences in the strain–stress response is due to the formation of R-phase in phase transformation that is not considered in our formulation. The differences in temperature distribution originated from the difference in the stress distribution, and also by considering the special specimen shape. The specimen has two thick bars attached to the ends for being mounted into the grips, and the heat transfer between the tube gage section and the attached parts to the tube at the ends is ignored in our theoretical modeling (see Fig. 1 in [19] for details of the specimen shape). As it is seen in Fig. 1(b), the specimen temperature immediately reaches the ambient temperature at the start of unloading, while this is not seen in the numerical simulations. This phenomenon may be caused by the high heat exchange between the specimen and the grips (that are in the same temperature with the ambient) that is ignored in the theoretical modeling.

4.2. Thermo-mechanical analysis of solid SMA bars subjected to pure torsion

As the first case study for analyzing the coupled thermo-mechanical response of solid SMA bars under torsion, consider an SMA bar with circular cross section of radius R=2.5 cm and length L=20 cm. The bar is made of a NiTi alloy with the following material properties: $E^A=72$ GPa, $E^M=30$ GPa, $\nu^A=\nu^M=0.42$, $\rho c^A=\rho c^M=2.6\times10^5$ J/(m^3 K), H=0.05, $\rho\Delta s_0=-0.42\times10^6$ J/(m^3 K), $A_f=281.6$ K, $A_s=272.7$ K, $M_f=238.8$ K, $M_s=254.9$ K. These properties are extracted for the phenomenological constitutive equations by Qidwai and Lagoudas [26] using the experimental date reported by Jacobus et al. [13] for a $Ni_{50}Ti_{50}$ alloy. The thermal conductivity is not reported for this material and we use k=18 W/(m K), which is reported in the literature for $Ni_{50}Ti_{50}$ [16]. The SMA bar is fixed at one end and the other end is twisted to the maximum twist angle per unit length of $\theta=5$ rad/m and then unloaded to the initial configuration at rest. The total loading–unloading time is assumed to be $\tilde{\tau}=10$ s. It is assumed that the whole bar is initially at the temperature $\hat{T}=300$ K and it is surrounded by still air with temperature $T_\infty=300$ K. The SMA specimen is vertical and surrounded by air with negligible flow speed. For calculating the free convection coefficient of a vertical cylinder, the empirical and numerical relations for the Nusselt number are used (see Section 5.1, and Fig. 2, Case III in [21], and also [12,25] for more details). By considering an average temperature difference of 15 K between the bar surface and the surrounding air, free convection coefficient for this case study is $h_\infty=4.5$ W/m^2 K (see Fig. 2, Case III in [21]). The number of grid points is M=50. The minimum time increment for having a stable solution in the explicit formulation is a function of the radius in each case study [24]. It is observed that in practice a convergence study is not required because the stable solution (with appropriate choice of time increment) always converges to the same stress and temperatures at the selected points and the only criterion is obtaining a smooth distribution that is acceptable by choosing 50 grid points. The results of this case study are depicted in Fig. 2. The shear stress distribution in the cross section of the bar in loading is shown in Fig. 2(a) for various twist angles.

Fig. 2(b) shows the shear stress distribution in the cross section for various twist angles in unloading. The observed spark in the shear stress distribution for $\theta=4$ rad/m is caused by the arrangement of different regions that experience phase transformation during loading and unloading. A detailed study of this phenomenon, along with some graphs showing the martensitic volume fraction distribution in the cross section are presented in Mirzaeifar et al. [20]. Since the temperature of the bar in the parts that experience phase transformation is above the austenite finish temperature during loading–unloading, there is no residual stress in the cross section at the end of unloading. It is worth noting that, temperature distribution in the cross section is affected by a set of parameters, e.g. the loading rate, size of the bar, and the ambient condition. Temperature may be lower than the initial temperature in some cases (see [21] and the following case studies in this paper). For having zero residual stress at the end of unloading, $\hat{T}>A_f$ is not an adequate condition and the complete history of temperature distribution in the cross section during loading–unloading should be considered. Fig. 2(c) shows the temperature distribution in the cross section of the bar during loading for various twist angles per unit length. There are some important observations regarding the temperature distribution worth explaining. As it is shown in Fig. 2(a), during loading for each twist angle the SMA bar has an austenite core surrounding the bar axis (characterized by a linear shear stress distribution in the cross section). Since there is no phase transformation inside this core, consequently no heat is generated in this region while the temperature of the material outside this austenite core is increased due to forward phase transformation. During loading, the temperature inside the austenite core is increasing by the hot

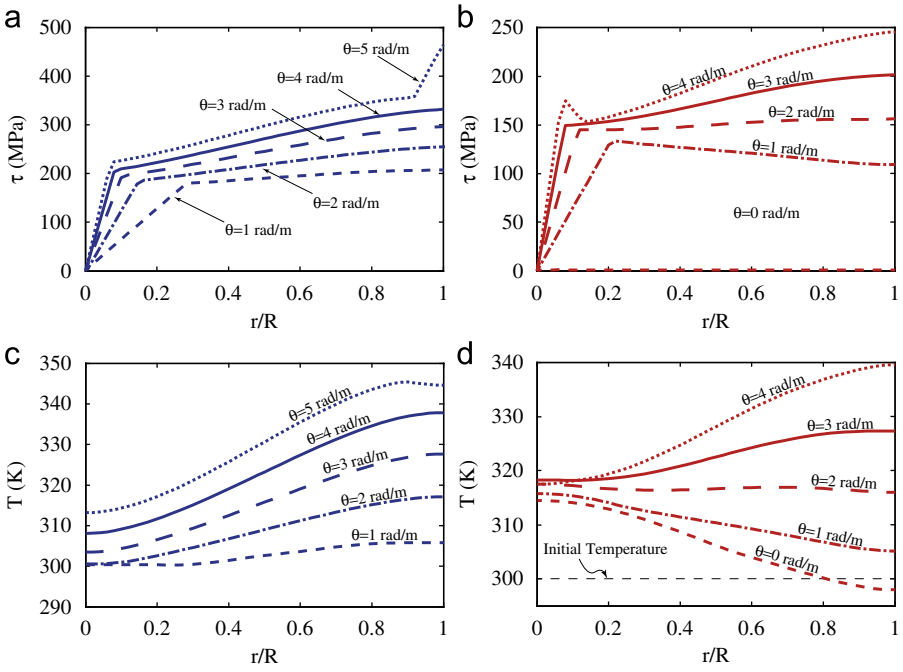

Fig. 2. Distributions of (a) shear stress during loading, (b) shear stress during unloading, (c) temperature during loading, and (d) temperature during unloading in the cross section of an SMA bar in free convection. The total loading–unloading time is $\tilde{\tau} = 10$ s.

material in the outer region due to thermal conduction. Because the temperature change inside this austenite core during loading and unloading is solely caused by the heat exchange with the outer material, as it will be shown in the sequel, temperature is strongly affected by the rate of loading and a complicated interaction between the loading rate and the core temperature is observed. This phenomenon will be studied in detail in the following case studies. The temperature distribution in the region attached to the outer radius at the end of loading phase ($\theta = 5$ rad/m) in Fig. 2(c) shows that the slope of temperature distribution changes at a specific point and temperature starts to decrease slightly in an annular ring attached to the outer surface. By looking at Fig. 2(a), it is seen that the material in this region is fully transformed to martensite (the linear part of shear stress distribution for the regions near $r/R = 1$). Since after completion of phase transformation there is no heat generation, the material in this region loses temperature due to heat exchange with the colder ambient at the surface. This negative slope in temperature distribution for the outer region is seen with more intensity for slower loading rates and higher convection coefficients as we will show in the following case studies. The temperature distribution during unloading in the cross section is depicted in Fig. 2(d) for various twist angles. As it is expected, the heat absorption during reverse phase transformation from martensite to austenite causes a temperature decrease in the cross section during unloading. The significance of the results in this figure is in predicting the temperature distribution in some regions at the end of unloading to be lower than the initial and ambient temperatures. This phenomenon is also observed in the uniaxial loading–unloading of SMA bars and a detailed study of this phenomenon in tension is presented in [21]. As it will be shown in the following case studies, temperature in the whole cross section may drop below the initial temperature for very slow loadings and high convection coefficients. This phenomenon will be further discussed in the sequel. It is worth noting that the thermo-mechanical coupled response is strongly affected by the strain history. The results presented in this paper correspond to a monotonic increase and decrease of twist angle. Any other loading or unloading history, e.g. a sinusoidal or impulsive loading, should be studied separately.

Another case study is considered in order to demonstrate the effect of loading rate on the response of SMA bars. The geometry, material properties, the initial condition, and the boundary conditions are the same as those of the previous example. The response of the bar is studied for four different loading rates $\tilde{\tau} = 1$, 10, 60, and 600 s ($\tilde{\tau}$ is the total loading–unloading time). For comparison purposes, the results of the exact solution of SMA bars assuming the whole material at a constant initial temperature during loading–unloading are also presented in this section. The shear stress distribution at the end of loading phase (SMA bar is twisted to $\theta = 5$ rad/m and then unloaded) in the cross section of the bar is shown in Fig. 3(a). As it is seen, the stress distribution is strongly affected by the loading rate. The slope of stress distribution in the region with $0 < \xi < 1$ is increased by increasing the loading rate.

The applied torque versus the twist angle for different loading rates is shown in Fig. 3(b). The loading rate does not have a significant influence on the applied torque for different loading rates for the present case in which the bar is subjected to free convection by air. We will show in the following examples that the effect of loading rate on the applied torque depends also on the boundary conditions and different results are observed for higher convection coefficients. Fig. 3(a) and (b) reveals a remarkable difference between both the stress distribution and applied torque of the present analysis and those obtained by considering the isothermal loading–unloading assumption. It is shown in these figures that considering the bar in the constant initial temperature during loading–unloading is unrealistic even for the slow loading cycle with $\tilde{\tau} = 600$ s. We will show in the next example that slow loading rate is not an adequate measure of the isothermal response of SMA bars in torsion; the ambient condition should be considered as well to justify the accuracy of assuming a constant temperature during loading–unloading. The temperature distribution in the cross section at the end of the loading phase is depicted in Fig. 3(c). As it is

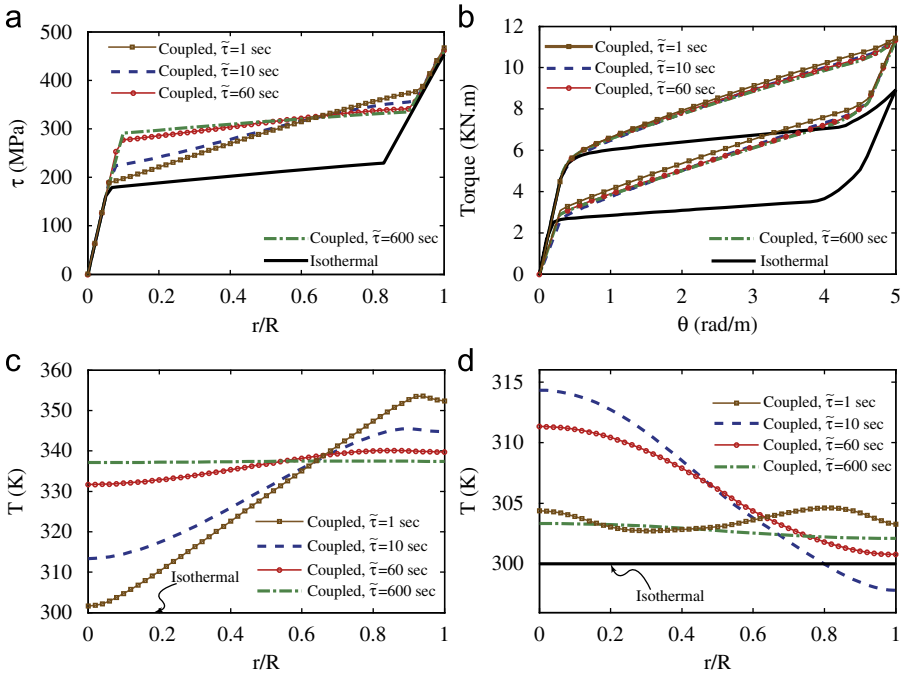

Fig. 3. The effect of loading rate on (a) shear stress distribution at the end of loading, (b) applied torque versus twist angle, (c) temperature distribution at the end of loading, and (d) temperature distribution at the end of unloading in the cross section of an SMA bar in free convection ($h_\infty = 4.5$ W/m^2 K).

shown, the slope of temperature distribution decreases for slower loading rates. This is expected because as explained earlier the temperature in the central austenite core, with no phase transformation heat generation, increases by the heat flux conducted from the outer region. For very fast loading (e.g. see $\tilde{\tau} = 1$ s in Fig. 3(c)), the generated heat in the outer regions does not have enough time to warm the central austenite core and hence the temperature at the center remains close to the initial temperature. For the slow loading $\tilde{\tau} = 600$ s, the temperature distribution is almost uniform. However, it is worth mentioning that this uniform temperature is not the same as that of an isothermal loading process (compare the temperature by assuming an isothermal loading with the slow loading in Fig. 3(c)). Temperature distribution in the cross section at the end of unloading phase is shown in Fig. 3(d). It is seen that the effect of loading rate on the temperature at the end of unloading is more complicated compared to the previous cases. Temperature distributions for $\tilde{\tau} = 1$ and 600 s are similar. This seems surprising at first. This figure clearly shows the complexity of the coupling between various parameters, e.g. loading rate and boundary conditions on the response of bars in torsion. For having a more precise understanding of the temperature changes during a loading–unloading cycle, and explaining the non-trivial results shown in Fig. 3(d), the history of temperature at the center of the bar is shown in Fig. 4.

Looking at Fig. 4 and also Fig. 3(c) and (d) leads to some important conclusions. As it is seen in Fig. 4, and as explained earlier, during fast loading the material at the center is not warmed by the outer material, and at the end of loading temperature at the center is remarkably lower than those of the outer parts (see Fig. 3(c)). The heat flux from the outer material toward the center in this case causes a slight temperature increase at the center during unloading as it is shown in Fig. 4. The whole process leads to a temperature slightly above the initial temperature at the end of unloading in fast loading. However, as shown in Fig. 4, for the slow loading rate of $\tilde{\tau} = 600$ s, there is enough time for the heat flux to warm the internal austenite core of the bar and the temperature at the center increases significantly during loading. At the end of loading the whole cross section is in an almost uniform high temperature (see Fig. 3(c)). During slow unloading, temperature of

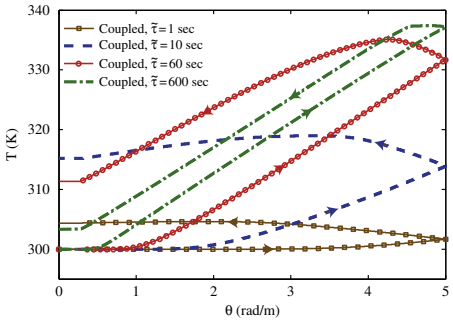

Fig. 4. The history of temperature at the center of an SMA bar subjected to pure torsion with free convection boundary condition for different loading rates.

the material in the outer parts decreases due to reverse phase transformation heat absorption and because unloading is slow there is enough time for the heat flux to cool down the material in the central parts of the cross section. As shown in Fig. 4 temperature at the end of unloading is slightly above the initial temperature and close to the final temperature in fast loading. Considering the four graphs presented in Fig. 4, it is seen that decreasing the loading rate from $\tilde{\tau} = 1$ s to $\tilde{\tau} = 600$ s, the slope of temperature changes during loading and unloading increases. Also it is seen that the area of the hysteretic temperature history increases from $\tilde{\tau} = 1$ s to $\tilde{\tau} = 60$ s and then decreases from $\tilde{\tau} = 60$ s to $\tilde{\tau} = 600$ s. For extremely fast and slow loadings, the hysteresis areas will be zero (based on the above-mentioned explanation for relatively fast and slow loadings $\tilde{\tau} = 1$ and 60 s).

In order to study the effect of various ambient conditions on the coupled thermo-mechanical response of SMA bars subjected to pure torsion, consider an SMA bar with the same initial conditions, material properties, and geometry as the previous case studies. The total loading–unloading time is $\tilde{\tau} = 600$ s and various ambient conditions are considered. For comparison purposes, the results of the exact solution assuming isothermal

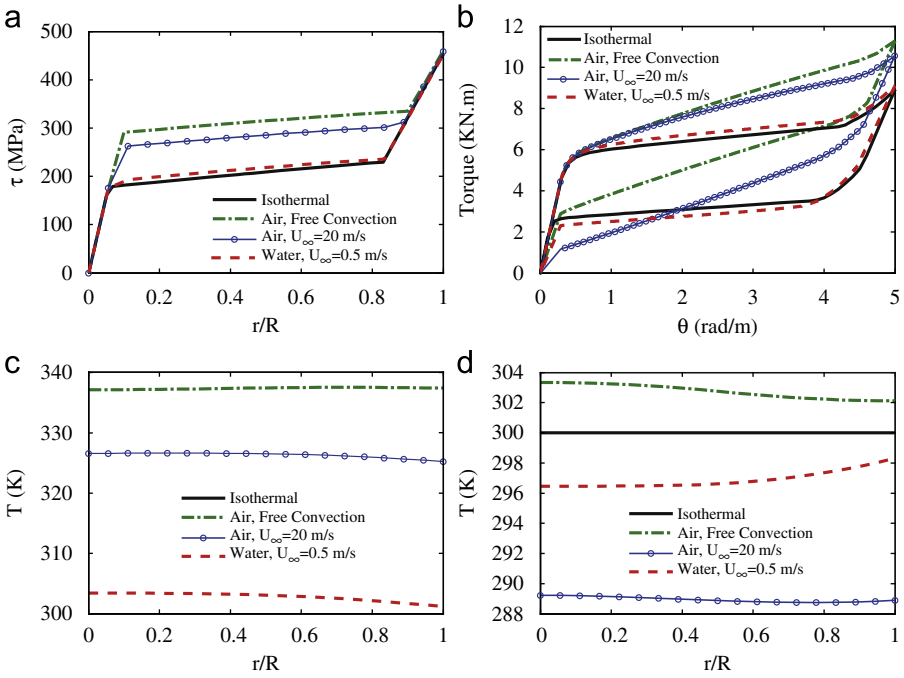

Fig. 5. The effect of ambient condition on (a) shear stress distribution at the end of loading, (b) applied torque versus twist angle, (c) temperature distribution at the end of loading, and (d) temperature distribution at the end of loading in the cross section of an SMA bar. The total loading–unloading time is $\tilde{\tau} = 600$ s.

loading–unloading are also presented here. In recent years SMA devices have been used in various structures ranging from buildings and bridges to aerospace structures [3,4,9]. The SMA devices in these structural applications are exposed to various ambient conditions, e.g. the slow air flow in buildings, fast air flow in aerospace structures, and water flow in bridges. In this case study we consider the free convection by air, forced convection by air flow with speed of $U_\infty = 20$ m/s, and water flow with the speed of $U_\infty = 0.5$ m/s, which is a common value for the speed of water in rivers (the average water velocity in rivers varies from 0.1 m/s to 3 m/s). Temperature of both air and water flows are assumed to be $T_\infty = 300$ K. Using the empirical relations for the forced convection (see [21] for details), the convection coefficients are obtained as $h_\infty = 91.71$ W/m^2 K for air flow and $h_\infty = 2529.3$ W/m^2 K for water flow. The convection coefficient for free air is $h_\infty = 4.5$ W/m^2 K as explained in the previous case studies. The SMA bar is twisted from rest (fully austenite material) to $\theta = 5$ rad/m and unloaded. The shear stress distribution in the cross section of the bar for different ambient conditions is shown in Fig. 5(a). It is seen that changing the boundary conditions causes moving of the shear stress plateau without a significant change in the slope (the slope of shear stress distribution varies by changing the loading rate as shown in Fig. 3(a)).

The applied torque versus the twist angle of the SMA bar is shown in Fig. 5(b). The most important observation in these figures is the deviation of the results corresponding to each ambient condition from the isothermal results. It is seen that although the loading–unloading is applied in 10 min, only the water flow ambient with a very large convection coefficient is giving similar results to those obtained by assuming a constant temperature during loading–unloading. We will study the effect of various parameters on the validity of isothermal assumption in Section 5. Temperature distribution at the end of loading is shown in Fig. 5(c). It is clearly seen that only for the SMA bar operating in water flow the temperature distribution remains constant and close to the initial temperature. For the other cases, although the temperature distribution is almost constant, it is remarkably higher than the initial temperature in the whole cross section.

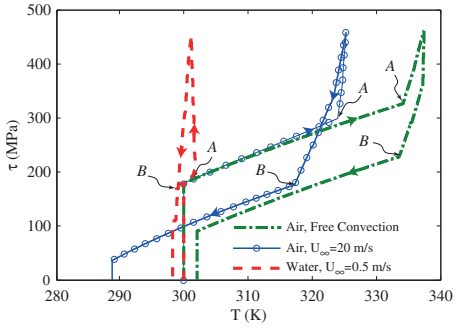

Fig. 6. Temperature versus shear stress at the surface of an SMA bar subjected to pure torsion for different ambient conditions. The total loading–unloading time is $\tilde{\tau} = 600$ s.

Both the temperature uniformity and temperature change with respect to the initial conditions are studied in Section 5 for various size, loading rate, and ambient conditions. The temperature distribution at the end of the unloading phase is depicted in Fig. 5(d). Two important observations are made: temperature in the whole cross section is lower than the initial and ambient temperatures for both the air and water flows, and temperature of the SMA bar exposed to air flow is lower than that of the bar exposed to water flow. These observations can be explained by studying the history of temperature during loading–unloading. The history of temperature at the outer surface of the bar is shown in Fig. 6. Temperature versus shear stress is shown in this figure to specify the different parts of loading–unloading phases before, during, and after phase transformation. In Fig. 6, the end of forward phase transformation is denoted by A and the start of reverse phase transformation is marked by the symbol B in all the graphs. We will use these special points in the sequel to explain more details of the material response during loading and unloading.

Starting from $T = \hat{T} = 300$ K the vertical part with no temperature change corresponds to the response of material at the surface

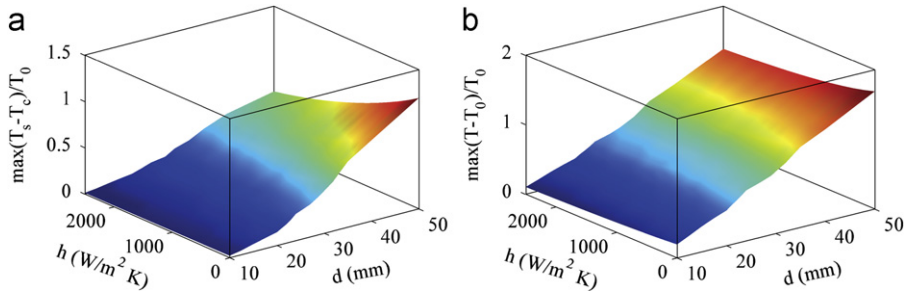

Fig. 7. The normalized maximum temperature difference between the surface and center (a), and the normalized maximum temperature increase with respect to the initial temperature (b) versus the convection coefficient and diameter ($T_0=27$ °C). The subscripts *s* and *c* represent the values measured at the surface and center of the bar, respectively.

before the start of forward phase transformation. This vertical plateau is proceeded by a temperature increase during forward phase transformation. The forward phase transformation continues up to the point *A* on all the graphs. As it is seen, with free convection boundary condition, temperature increases remarkably during phase transformation, while with the water flow boundary condition it remains almost constant during this phase. The amount of temperature increase during phase transformation at the surface of the SMA bar in air flow is between the other two boundary conditions. After point *A*, the phase transformation at the surface is completed and the material is fully transformed to martensite. With further loading, there is no phase transformation heat generation at the surface. At this stage of loading (from the end of phase transformation at *A* to the end of loading), the material at the surface loses temperature due to cooling by the ambient, and gaining heat by conduction from the inner parts that are experiencing forward phase transformation. For the free and forced convection of air, the conduction from inner parts is dominant and the temperature at the surface increases, while for the water flow, cooling by the ambient is dominant and temperature at the surface decreases slightly. The unloading phase starts with an elastic stage up to point *B*. In this stage, the reverse phase transformation does not occur. On the other hand, the material is exposed to an ambient that is cooling the bar. In all the cases, temperature decreases at the surface during this stage of unloading. For the free convection boundary condition, temperature deceases slightly while temperature at the surface of the bar exposed to force convection by air decreases much more. Temperature of bars exposed to water flow does not change much during this stage because the material is not heated too much during loading and the temperature is almost equal to the ambient temperature. This elastic unloading stage is proceeded by the reverse phase transformation from martensite to austenite at the surface and is accompanied by heat absorption. For the free convection case for which the temperature drop during the elastic unloading phase was negligible, the heat absorption during reverse phase transformation returns the temperature near the initial temperature at the end of unloading. However, for the forced air convection for which temperature dropped remarkably, the reverse phase transformation heat absorption causes the material to be at a lower temperature compared to the initial and ambient temperatures at the end of unloading. For the water flow, the high convection coefficient keeps the material temperature close to the ambient temperature during the whole unloading phase (heat flux is from the ambient to the material for overcoming the heat absorption during the reverse phase transformation). Temperature distributions at the end of unloading depicted in Fig. 5(d) are now clearly understood and temperature history shown in Fig. 6 explains the reason for observing the lowest temperature for the forced air flow convection. A detailed study of the effect of ambient condition on the temperature history during loading–unloading and a precise study of the conditions required for observing a temperature distribution below the initial temperature is presented by the authors for SMA bars and wires subjected to uniaxial tension in [21].

The presented results clearly show the necessity of using a coupled thermo-mechanical formulation for analyzing torsion of SMA bars. Even for relatively slow loadings, considering the whole material in a constant temperature is not a realistic assumption (see Fig. 3(a) and (b), and also Section 5 for a detailed study of the effect of various parameters on the maximum temperature gradient). As it is shown in [20,22], in general, the cross section of a bar in pure torsion is divided into three regions during both loading and unloading. During loading, the inner region is fully austenite, the outer region is fully transformed into martensite, and the phase transformation is happening in the intermediate region. During unloading, the inner austenite region unloads elastically and the rest of cross section is divided into two regions. In one of these two regions, the material has been partially transformed to martensite during loading but the reverse phase transformation has not started yet and in the other region the material has experienced both forward and reverse phase transformations [20]. Note that phase transformation occurs in only one of these three regions. Consequently, heat is generated or absorbed in only one region. As a result, a complicated thermo-mechanical problem should be solved considering the heat flux between these three regions and also the ambient condition. Existence and interaction of these three regions in the cross section causes a more complex temperature distribution in the cross section compared to that of the uniaxial case. This non-uniform temperature distribution is the origin of the significant differences in the stress distributions that are observed between the coupled thermo-mechanical and isothermal torsion solutions.

5. Effect of size, boundary conditions, and loading rate on the temperature distributions in the cross section

The main effect of thermo-mechanical coupling is reflected in the temperature changes, although this temperature change affects the other parameters including the stress and martensitic volume fraction as well. In order to study the thermo-mechanical coupling effects, two different parameters are considered in this section: the maximum temperature difference between the surface and center in the cross section, and the maximum temperature change with respect to the initial temperature. We will consider only the loading phase in this section, and the maximum is calculated by comparing all the increments during loading. In some cases the temperature distribution is excessively non-uniform as seen in Figs. 2 and 3. In some other cases, the temperature distribution in the cross section may be approximately uniform,

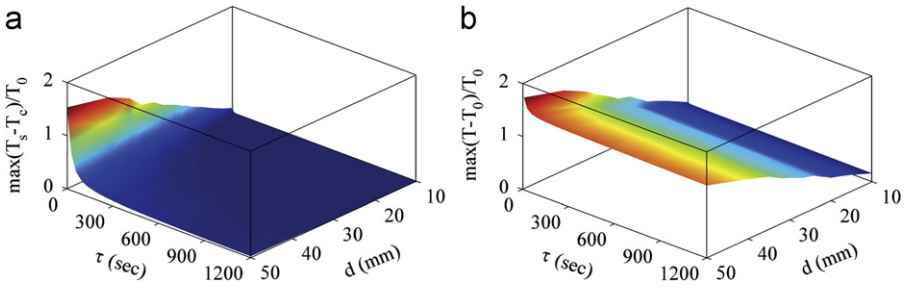

Fig. 8. The normalized maximum temperature difference between the surface and center (a), and the normalized maximum temperature increase with respect to the initial temperature (b) versus the loading rate and diameter (T_0=27 °C). The subscripts *s* and *c* represent the values measured at the surface and center of the bar, respectively.

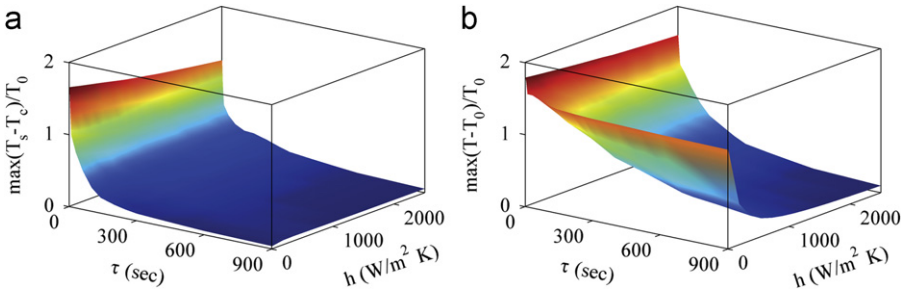

Fig. 9. The normalized maximum temperature difference between the surface and center (a), and the normalized maximum temperature increase with respect to the initial temperature (b) versus the loading rate and convection coefficient (T_0=27 °C). The subscripts *s* and *c* represent the values measured at the surface and center of the bar, respectively.

while the temperature in the whole cross section is remarkably different from the initial temperature (e.g. the case shown in Fig. 5). As shown in the previous sections, the accuracy of assuming an isothermal loading-unloading for SMA bars subjected to torsion strongly depends on the ambient conditions, size, and loading rate. In this section we consider the maximum temperature difference between the surface and center in the cross section, and the maximum temperature change with respect to the initial temperature as a measure of the thermo-mechanical coupling effect on the response of the bar. In other words, when both these parameters are small, the bar subjected to torsion can be assumed isothermal during loading–unloading with an acceptable accuracy.

As the first case study in this section, the effect of convection coefficient and diameter on the temperatures is studied in Fig. 7. In this case study, the total loading–unloading time is $\tau = 10$ s. Both the considered parameters increase with a steep slope by increasing the diameter. Fig. 7(a) shows that for large diameters, increasing the convection coefficient decreases the temperature gradient between the surface and center. However, as shown in Fig. 7(b), the temperature is much higher than the initial temperature even for large convection coeffcients, when the diameter is large. It can be concluded that for this loading rate, the isothermal assumption is valid only for small diameters, i.e. SMA wires.

The effect of loading rate and diameter on the temperature distribution in loading phase is studied in Fig. 8 for a bar subjected to free convection of air. The maximum temperature difference between the surface and center during loading is small for slow loading rates even for large bars (Fig. 8(a)). However, as shown in Fig. 8(b), the maximum temperature increase with respect to the initial temperature is negligible only for small diameters.

The effect of loading rate and convection coefficient on the temperature distributions is studied in Fig. 9 for a thick bar (d=5 cm). As shown in Fig. 9(a), the maximum temperature difference between the surface and center during the loading phase uniformly decreases by decreasing the loading rate for all the convection coefficients. Fig. 9(b) shows that the maximum temperature difference with respect to the initial temperature is negligible only when both loading time and convection coefficient are large enough.

6. Conclusions

In this paper, the effect of heat generation and absorption during phase transformation in analyzing the pure torsion of shape memory alloy bars with circular cross sections is studied. A coupled thermo-mechanical formulation is presented for SMA bars by coupling the energy balance in the presence of heat flux with our previous exact solution of SMA bars in torsion. Using the present formulation one is capable of calculating the non-uniform temperature distribution in the cross section caused by the generation and absorption of heat due to phase transformation, the heat conduction in the cross section, and the heat exchange with the ambient at the outer surface. It is shown that the response of SMA bars in torsion is strongly time dependent as the heat flux in the cross section and the heat exchange with the ambient is affected by the rate of loading. Several numerical case studies are presented in order to show the necessity of considering the coupled thermo-mechanical formulation by comparing the results of the present model with those obtained by assuming that the whole cross section is in a constant temperature during loading–unloading. Pure torsion of SMA bars in various ambient conditions subjected to different loading–unloading rates are studied and it is shown that the isothermal solution gives inaccurate results for most practical ambient conditions and loading rates.

References

[1] J.G. Boyd, D.C. Lagoudas, Thermodynamical constitutive model for shape memory materials. Part I. The monolithic shape memory alloy, International Journal of Plasticity 12 (6) (1996) 805–842.

[2] B.C. Chang, J. Shaw, M. Iadicola, Thermodynamics of shape memory alloy wire: modeling, experiments, and application, Continuum Mechanics and Thermodynamics 18 (2006) 83–118.
[3] R. DesRoches, M. Delemont, Seismic retrofit of simply supported bridges using shape memory alloys, Engineering Structures 24 (3) (2002) 325–332.
[4] R. DesRoches, B. Taftali, B.R. Ellingwood, Seismic performance assessment of steel frames with shape memory alloy connections. Part I. Analysis and seismic demands, Journal of Earthquake Engineering 14 (4) (2010) 471–486.
[5] M. Dolce, D. Cardone, Mechanical behaviour of shape memory alloys for seismic applications. I. Martensite and austenite NiTi bars subjected to torsion, International Journal of Mechanical Sciences 43 (11) (2001) 2631–2656.
[6] Y. Dong, Z. Boming, L. Jun, A changeable aerofoil actuated by shape memory alloy springs, Materials Science and Engineering: A 485 (2008) 243–250.
[7] G.E. Forsythe, M.A. Malcolm, C.B. Moler, Computer Methods for Mathematical Computations, Prentice-Hall, 1976.
[8] H.G. Grewe, E. Kappler, Über die ermittlung der verfestigungskurve durch den torsionsversuch an zylindrischen vollstäben und das verhalten von vielkristallinem kupfer bei sehr hoher plastischer schubverformung, Physica Status Solidi (b) 6 (2) (1964) 339–354.
[9] D.J. Hartl, D.C. Lagoudas, Aerospace applications of shape memory alloys, Proceedings of the Institution of Mechanical Engineers, Part G: Journal of Aerospace Engineering 221 (4) (2007) 535–552.
[10] P. Henrici, On helical springs of finite thickness, The Quarterly of Applied Mathematics XIII 11 (1955) 106–110.
[11] T.J. Higgins, A comprehensive review of Saint-Venant's torsion problem, American Journal of Physics 10 (5) (1942) 248–259.
[12] J. Holman, Heat Transfer, seventh ed., McGraw-Hill, New York, 1990.
[13] K. Jacobus, H. Sehitoglu, M. Balzer, Effect of stress state on the stress-induced martensitic transformation in polycrystalline Ni–Ti alloy, Metallurgical and Materials Transactions A 27 (1996) 3066–3073.
[14] L.M. Kachanov, Foundations of the Theory of Plasticity, North-Holland Publishing Company, 1971.
[15] H.S. Kim, Finite element analysis of torsional deformation, Materials Science and Engineering: A 299 (1–2) (2001) 305–308.
[16] D.C. Lagoudas, Shape Memory Alloys: Modeling and Engineering Applications, Springer, New York, 2008.
[17] C.Y. Leea, H.C. Zhuob, C.W. Hsu, Lateral vibration of a composite stepped beam consisted of SMA helical spring based on equivalent Euler–Bernoulli beam theory, Journal of Sound and Vibration 324 (2009) 179–193.
[18] T. Lim, Behavior of a Ni–Ti Shape Memory Alloy Under Cyclic Proportional and Nonproportional Loading, Ph.D. Thesis, Georgia Institute of Technology, Atlanta, Georgia, 1999.
[19] T.J. Lim, D.L. McDowell, Mechanical behavior of an Ni–Ti shape memory alloy under axial–torsional proportional and nonproportional loading, Journal of Engineering Materials and Technology—Transactions of the ASME 121 (1) (1999) 9–18.
[20] R. Mirzaeifar, R. Desroches, A. Yavari, Exact solutions for pure torsion of shape memory alloy circular bars, Mechanics of Materials 42 (8) (2010) 797–806.
[21] R. Mirzaeifar, R. Desroches, A. Yavari, Analysis of the rate-dependent coupled thermo-mechanical response of shape memory alloy bars and wires in tension, Continuum Mechanics and Thermodynamics 23 (4) (2011) 363–385.
[22] R. Mirzaeifar, R. Desroches, A. Yavari, A combined analytical, numerical, and experimental study of shape-memory-alloy helical springs, International Journal of Solids and Structures 48 (3–4) (2011) 611–624.
[23] A. Nadai, Theory of Flow and Fracture of Solids I, McGraw-Hill, New York, 1950.
[24] M.N. Özişik, Finite Difference Methods in Heat Transfer, CRC-Press, Boca Raton, FL, 1994.
[25] C.O. Popiel, Free convection heat transfer from vertical slender cylinders: a review, Heat Transfer Engineering 29 (6) (2008) 521–536.
[26] M.A. Qidwai, D.C. Lagoudas, On thermomechanics and transformation surfaces of polycrystalline NiTi shape memory alloy material, International Journal of Plasticity 16 (10) (2000) 1309–1343.
[27] J.A. Shaw, S. Kyriakides, Thermomechanical aspects of NiTi, Journal of the Mechanics and Physics of Solids 43 (8) (1995) 1243–1281.
[28] J.C. Simo, T.J.R. Hughes, Computational inelasticity. in: Interdisciplinary Applied Mathematics, vol. 7, Springer-Verlag, New York, 1998.
[29] I.S. Sokolnikoff, Mathematical Theory of Elasticity, McGraw-Hill, New York, 1956.
[30] M. Speicher, D.E. Hodgson, R. DesRoches, R.T. Leon, Shape memory alloy tension/compression device for seismic retrofit of buildings, Journal of Materials Engineering and Performance 18 (2009) 746–753.
[31] F. Székely, I. Groma, J. Lendvai, Nonlocal effects in torsional deformation, Materials Science and Engineering: A 277 (1–2) (2000) 148–153.
[32] A.M. Wahl, Mechanical Springs, Penton Publishing Company, Cleveland, USA, 1944.